Journal of Colloid and Interface Science 533 (2019) 13–23

Contents lists available at ScienceDirect

Journal of Colloid and Interface Science

journal homepage: www.elsevier.com/locate/jcis

Regular Article

Long-term antibacterial stable reduced graphene oxide nanocomposites loaded with cuprous oxide nanoparticles

Zhaoqing Yang [a], Xiangping Hao [a], Shougang Chen [a,*], Zhenqing Ma [a], Wenhui Wang [a], Caiyu Wang [a], Longfei Yue [a], Haiyun Sun [a], Qian Shao [b], Vignesh Murugadoss [c], Zhanhu Guo [c,*]

[a] School of Materials Science and Engineering, Ocean University of China, Qingdao 266100, China
[b] College of Chemical and Environmental Engineering, Shandong University of Science and Technology, Qingdao 266590, China
[c] Integrated Composites Laboratory (ICL), Department of Chemical & Biomolecular Engineering, University of Tennessee, Knoxville, TN 37996, USA

GRAPHICAL ABSTRACT

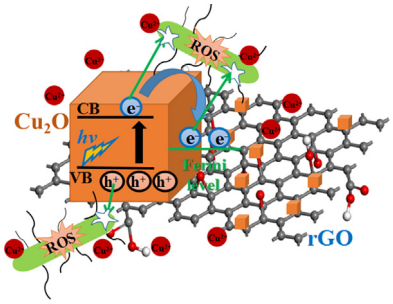

ARTICLE INFO

Article history:
Received 20 June 2018
Revised 2 August 2018
Accepted 17 August 2018
Available online 18 August 2018

Keywords:
rGO-Cu_2O nanocomposites
Long-Term
Antibacterial

ABSTRACT

Stable reduced graphene oxide-cuprous oxide (rGO-Cu_2O) nanocomposites with long-term antibacterial activities were prepared by reducing copper sulfate supported on GO using ascorbic acid as reducing agent in the presence of polyethylene glycol (PEG) and sodium hydroxide at room temperature. The rGO provided a protective barrier for Cu_2O, preventing Cu_2O from reacting with external solution to leach copper ions too quickly. Meanwhile, the rGO also promoted the separation of photoexcited charge carriers of Cu_2O nanoparticles to enhance the oxidative stress reactive and protected Cu_2O from falling apart in the phosphate buffered solution (PBS) solution to prolong the generation time of reactive oxygen species (ROS). More importantly, the large specific surface area of rGO improved the dispersibility of Cu_2O by electrostatic interaction. The synergistic effect of sustained release of copper ions, elevated ROS production ability and uniform dispersion of rGO-Cu_2O nanocomposites resulted in the excellent antibacterial activities of rGO-Cu_2O nanocomposites against *Escherichia coli* (*E. coli*) and *Staphylococcus aureus* (*S. aureus*) which were maintained around 70% and 65% and were increased by 40% and 35% compared with free Cu_2O after immersing 30 days in PBS solutions.

1. Introduction

Microorganisms, easily found in the ocean, air and soil, will form a biofilm and have a great impact on human activities. The presence of biofilm will cause not only corrosion in metal surfaces in industrial process, but also the hygiene and safety issues when bacteria are involved in the food industry, and the device-related infections in medical fields [1–3]. Therefore, antibacterial agents play an important role in our life. However, traditional bactericides gradually lose their bactericidal effects when bacteria develop their own resistance. Thereby, more attentions have been focused on the

* Corresponding authors.
E-mail addresses: sgchen@ouc.edu.cn (S. Chen), zguo10@utk.edu (Z. Guo).

https://doi.org/10.1016/j.jcis.2018.08.053
0021-9797/

exploration of new antibacterial agents like polymer and nanosized inorganic materials [4–6].

Recently, copper related materials attract growing attentions because of their wide potential applications such as hydrogen production, solar energy, catalysis, and anode materials for lithium ion batteries [7–12]. Especially, cuprous oxide (Cu_2O), as a potential and widely abundant, comparatively cheap bactericide, has been extensively used in the fields of antibacterial. Cu_2O can kill bacteria by means of releasing copper ions and producing reactive oxygen species (ROS) on the surface when contact with bacteria [13]. Therefore, the antibacterial ability of Cu_2O is associated with the morphology (size and shape), release properties of copper ion and dispersion closely. For example, Feng et al. studied the cytotoxicity of Cu_2O with different morphologies [14]. Their research showed that small cubic Cu_2O crystal with the most exposed (1 0 0) crystal plane had the best bactericidal performance. Because ROS was mainly generated on the (1 0 0) crystal plane, the larger the specific surface area was, the more likely the Cu_2O would fall apart to release copper ion to kill bacterial. Although Cu_2O has shown immediate antibacterial properties, Cu_2O will be deteriorated after a short period of use due to rapid release of copper ions and easy aggregation. Hence, it is crucial to find a proper support material to improve the long-term antimicrobial performance.

Carbon materials such as graphene oxide (GO), reduced graphene oxide (rGO), carbon nanotubes and graphitic carbon nitride nanosheets have initiated a large number of scientific activities in physics, biology, electronics and chemistry fields [15–25]. It is greatly promising to exploit the graphene nanosheets as a support material for metal oxide nanoparticles to form hybrid nanocomposites due to their unique two-dimensional (2-D) nanostructure and extraordinary properties like high thermal conductivity, high electron mobility of $2 \times 10^5\ cm^2\ V^{-1}\ s^{-1}$ and tremendous specific surface area of 2965 $m^2\ g^{-1}$ [26–28]. For example, Shao et al. used graphene to improve the dispersion of nano-silver and prepared GO-Ag composites which showed excellent antibacterial activities [29]. Lei et al combined graphene with ZnS to improve the abilities to separate the photoexcited charge carriers from ZnS composites for superior photoelectric applications due to electron capture and transfer ability of graphene [30]. Thus, the ability of GO dispersing nanoparticles can be used to prevent Cu_2O from aggregating. The ability of separating photogenerated carriers can be used to promote Cu_2O to cause a stronger oxidative stress reactive with the effect of destroying the balance between oxidation and antioxidation in the cell and thus resulting in cell death. Because oxidative stress reactive happened in a process that the photoexcited electrons of Cu_2O reacted with O_2 to generate super-oxide radical anions ($\cdot O^{2-}$) and hydrogen peroxide (H_2O_2) for further killing the bacteria or the photoexcited electrons and holes of Cu_2O directly attacked the bacterial cells themselves [31].

Cu_2O can interact with GO nanosheets through physisorption, electrostatic binding or charge-transfer interactions because there are many hydroxyl, epoxide, carbonyl, and carboxyl groups on the basal planes of GO [32]. Additionally, Cu_2O was reduced on the surface of GO nanosheets, forming a stable rGO-Cu_2O nanocomposite. The rGO-Cu_2O nanocomposites have better bactericidal properties than Cu_2O, because the "blade like edges" of rGO can damage bacterial cell membranes physically, and the rGO nanosheets with a lower Fermi potential level can promote Cu_2O to generate more ROS, which exerts synergistic bactericidal [33]. Most important, the aggregation of Cu_2O can be prevented after the incorporation of rGO because rGO has a large specific surface area and provides strong attachment sites for Cu_2O. At the same time, rGO protects Cu_2O from reacting with external solution to disintegrate and releasing copper ion quickly. The dispersion and copper ion release rate are crucial for long-lasting antibacterial properties of Cu_2O.

Herein, rGO nanocomposites loaded with cubic Cu_2O nanoparticles were prepared by a simple wet chemical method at room temperature. The release of copper ions and dispersion properties of rGO-Cu_2O were studied by means of inductively coupled plasma (ICP) and stability experiment. The reactive oxygen species assay kit was used to assess the ROS production effect of rGO, Cu_2O and rGO-Cu_2O. The long-lasting antibacterial properties of Cu_2O and rGO-Cu_2O were investigated by plate colony counting method after storing in PBS solutions for different time intervals. The copper ion release properties, ROS generation performance and dispersion of rGO-Cu_2O were studied. The exhibited better and long-term bacteriostatic for rGO-Cu_2O was disclosed considering the synergistic effects of these three aspects, i.e., copper ion release properties, ROS generation performance and dispersion.

2. Experimental

2.1. Materials

Graphite powder, 37% hydrochloric acid (HCl), 98% sulfuric acid (H_2SO_4), 85% phosphoric acid (H_3PO_4), 30% hydrogen peroxide (H_2O_2), L-ascorbic acid, Sodium Chloride (NaCl) and Yeast Extract were purchased from Sinopharm Chemical Regent Co. Ltd. (shanghai, China). Potassium permanganate ($KMnO_4$), cupric sulfate ($CuSO_4{\cdot}5H_2O$), sodium hydroxide (NaOH), poly-ethylene oxide (av. MW 600; also called polyethylene glycol), absolute ethyl alcohol and Peptone were supplied by Tianjin bodi chemical Co. Ltd. All chemicals reagents were analytical grade and used as-received without any further purification in this work. Ultrapure deionized water was used for all solution preparation. Phosphate-buffered saline (PBS, pH 6.2) solutions were stored at 4 °C after high pressure steam sterilization. Reactive Oxygen Species Assay Kit was purchased from Beyotime (Hainan, China). *E.coli* (ATCC25922) and *S. aureus* (ATCC25923) were provided by Rishui Biotech Co. Ltd (Qingdao, China).

2.2. Synthesis of GO

Graphene oxide (GO) was prepared according to the reported procedures [34]. Briefly, a mixture of H_2SO_4/H_3PO_4 (360:40 mL) was added to the mixture of graphite flakes (3.0 g) and $KMnO_4$ (18.0 g). The reaction was heated to 50 °C and stirred for 14 h, and then cooled down to room temperature and poured into ice water (about 400 mL). Subsequently, 30% H_2O_2 was added to the mixture till it turned bright yellow. The mixed solution was then centrifuged and the precipitation was put in the vacuum freeze dryer for 24 h.

2.3. Synthesis of Cu_2O

Three kinds of cuprous oxide nanoparticles (Cu_2O NPs) were synthesized according to three different procedures [35], which could be seen at supporting information (Experimental). The prepared Cu_2O samples had been characterized by TEM (Fig. S1). Fig. S1 depicts that cubic Cu_2O with a size of 25 nm, cubic Cu_2O with a size of 150 nm and irregular Cu_2O with a size of 25 nm were synthesized successfully by procedure A, procedure B and procedure C, respectively. The XRD patterns of different morphologies and the sizes Cu_2O nanoparticles were shown in Fig. S2. The XRD characteristic diffraction peaks of three kinds of Cu_2O samples were in good agreement with the standard file of Cu_2O (JCPDS No. 05-0667) [36], indicating the successful preparation of Cu_2O nanoparticles. The antibacterial activities of the cubic Cu_2O nanoparticles with a size of 25 nm were superior than that of cubic Cu_2O with a size of 150 nm and irregular Cu_2O with a size of 25 nm

(Fig. S3 and Fig. S4). Because the number of colonies of cubic Cu_2O nanoparticles with a size of 25 nm was the least (Fig. S3) and the number of dead red bacteria of cubic Cu_2O nanoparticles with a size of 25 nm was the most (Fig. S4). Cubic Cu_2O nanoparticles with a size of 25 nm were selected to combine with rGO to form the nanocomposites for further study of long-term antibacterial properties.

Supplementary data associated with this article can be found, in the online version, at https://doi.org/10.1016/j.jcis.2018.08.053.

2.4. Preparation of rGO-Cu_2O nanocomposites

In brief, 2 mg GO was added into 40 mL 0.01 M copper (II) sulfate solution and was smashed for 15 min by Ultrasonic Cell Disruptor. Then the mixed solution was stirred for another 30 min to make sure that Cu^{2+} was absorbed onto GO sheets. The following preparation process was similar to that of procedure A: 10 mL 0.5 M PEG-600 stock solution was added to solution, and then 10 mL 0.1 M ascorbic acid and 30 mL 0.5 M NaOH were added dropwise to the solution simultaneously. The whole solution was kept stirring for another 5 min, afterward was remained undisturbed under nitrogen for 30 min to allow the reaction to complete at room temperature. The prepared products were defined as rGO-Cu_2O nanocomposites (Fig. 1).

2.5. Characterizations

The dried powders were characterized by X-ray diffraction (XRD) on a Bruker D8 Advance diffractometer with Cu Ka radiation to determine the crystal structure. The X-ray photoelectron spectroscopy (XPS, ESCALAB 250Xi, Thermo Fisher Scientific) data fitting was conducted on a Thermo Advantage. The photoluminescence (PL) spectra were analyzed by a fluorescence spectrophotometer (F-4600, Hitachi, Japan). The copper content was analyzed by a Thermogravimetric Analysis (TGA, METTLER TOLEDO TGA/DSC1/1600). Transmission electron microscopy (TEM) analyses was taken with a JEOL JEM2100 microscope. Copper ion release test was carried out on an ICAP-6300 Plasma emission spectrometer. Zeta potential was taken with a Zetasizer3000HS laser particle size analyzer. The component analysis of different samples were determined by the Ultraviolet and visible spectrophotometer (UV–vis) U-3900H manufactured by Hitachi Ltd and Fourier transform infrared spectroscopy (FTIR) IS-50 spectrometer (Nicolet, America) with KBr discs. The samples loaded with fluorescent probe 2′, 7′-dichlorofluorescein diacetate (DCFH-DA) were observed with a confocal laser scanning microscope (ZEISS Scope. A1).

2.6. Zeta potential test

The three prepared samples, i.e., Cu_2O, GO and rGO-Cu_2O were dispersed in ultrapure water to make 0.01 mg/mL solution respectively. 3 mL of each sample was taken by pipette to analyze the zeta potential.

2.7. Stability test

3 mg Cu_2O, GO and rGO-Cu_2O samples were added into 6 mL ultrapure water respectively and dispersed under ultrasonication. The optical images of different suspensions were taken after standing for 0 day, 1 day, 3 days, 7 days, 14 days and 30 days to observe their dispersion at room temperature.

2.8. Releasing properties of copper ions

The 40 μg/mL Cu_2O and rGO-Cu_2O were filtered after shaking 0 day, 1 day, 3 days, 7 days, 14 days and 30 days respectively in the PBS solution at room temperature. The solution was studied by ICP to evaluate the releasing properties of copper ions.

2.9. Reactive oxygen species (ROS) determination

Intracellular ROS generation was detected by reactive oxygen species assay kit. Before experiments, the fluorescent probe 2′,7′-dichlorofluorescein diacetate (DCFH-DA) was diluted 10^4 times with fluid medium prepared by mixing yeast extract (0.25 g), peptone (0.5 g), sodium chloride (NaCl, 0.25 g) with 50 mL Ultrapure deionized water. The rGO, Cu_2O and rGO-Cu_2O were dried after immersing in PBS for 0 day, 1 day, 3 days, 7 days, 14 days and 30 days to investigate the production of ROS in bacterial cell. 20 μL activated bacteria was distributed into 50 mL fluid medium containing 2 mg three kinds of prepared samples which were stored for 0 day, 1 day, 3 days, 7 days, 14 days and 30 days, respectively. All the samples were shaken 30 s to promote the production of ROS before loaded with 10 μM fluorescent probe DCFH-DA. DCFH-DA can passively diffuse into the cells and be deacetylated by esterase to form non-fluorescent 2,7-dichlorofluorescein (DCFH). In the presence of ROS, DCFH reacts with ROS to form the fluorescent product DCF, which was detected by a confocal laser scanning microscope after 30 min of incubation at 37 °C.

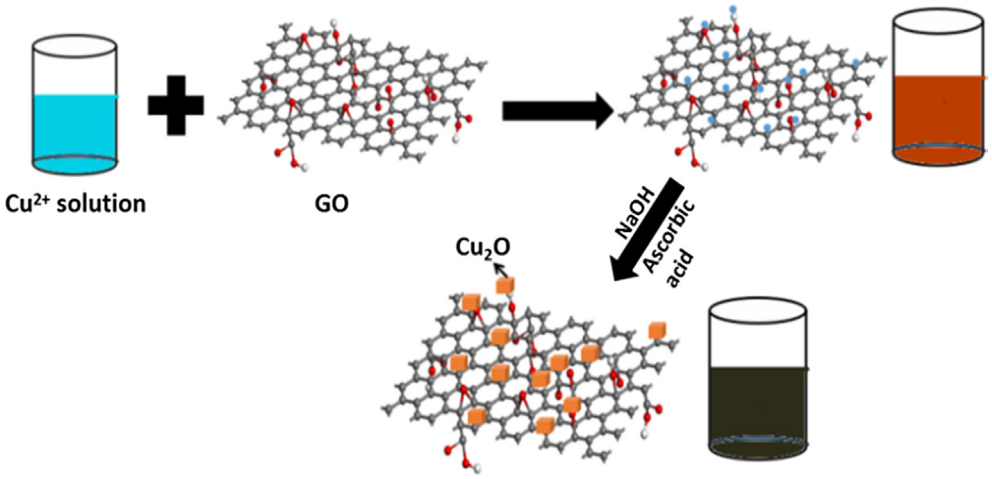

Fig. 1. Schematic illustration of the rGO-Cu_2O nanocomposite synthesis.

2.10. Long-term antibacterial activities assay

The antimicrobial ability of rGO-Cu_2O and Cu_2O was investigated by the plate colony counting method. The *E. coli* and *S. aureus* were selected as the test strains. All stuffs used in the antibacterial activity test needed be sterilized in an autoclave and the experimental operations were conducted in the super clean bench. The Cu_2O and rGO-Cu_2O were dried after immersing in PBS for 0 day, 1 day, 3 days, 7 days, 14 days and 30 days to investigate the change of antibacterial effectiveness. The *E.coli* and *S. aureus* should be activated. Breifly, 20 μL strains of bacteria were transferred to 50 mL fluid medium and were cultured for 20 h. Secondly, the activated bacteria needed be distributed into 50 mL fluid medium containing 2 mg Cu_2O nanoparticles, 2 mg rGO-Cu_2O nanocomposites and nothing as blank sample respectively for another 20-hour cultivation. All kinds of bacterium solutions were diluted to 10^4 times and 20 μL diluted Cu_2O, rGO-Cu_2O and blank solutions were layered over Luria-Bertani (LB) agar plates uniformly. The antibacterial activities of these materials could be observed through the number of colony after a period of time. All tests were repeated at least three times. The percentage of the bacterial reduction of each sample was calculated according to Eq. (1) [16]:

$$B_R = (A - B)/A \times 100\% \quad (1)$$

where B_R is the bacteriostatic percentage, A is the number of viable bacteria of the control group, and B is the number of viable bacteria of the experimental group.

3. Results and discussion

3.1. Characterization of GO, Cu_2O nanoparticles and rGO-Cu_2O nanocomposites

Fig. 2a shows the XRD patterns of pristine graphite (PG) and graphene oxide (GO). Compared to that of PG, the X-ray (0 0 2) peak of GO shifted from 26.7° to 11.4°, indicating the increased interlayer distance due to the introduction of various oxygenic functional groups (epoxy, hydroxyl, carboxyl and carbonyl) on both sides and edges of carbon sheets [37]. These oxygen functional groups can improve the hydrophilic properties of GO and become the attachment sites for cupric ions subsequently. Fig. 2b shows the XRD patterns of Cu_2O nanoparticles and rGO-Cu_2O nanocomposites. The strong diffraction peaks of the prepared Cu_2O at $2\theta = 29.65°$, 36.52°, 42.42°, 61.54°, 73.72° and 77.61° belong to the (1 1 0), (1 1 1), (2 0 0), (2 2 0), (3 1 1) and (2 2 2) crystal planes of Cu_2O, respectively, which are in good agreement with the standard file of Cu_2O crystals in cubic phase (JCPDS No. 05-0667) [36]. As for the line of Cu_2O-rGO, all the diffraction peaks are similar to those of pure Cu_2O (JCPDS No. 05-0667) while the characteristic peaks corresponding to the graphitic structure cannot be observed in the XRD curve of rGO-Cu_2O. The reason for these phenomena was that the aggregation and restacking of these prepared graphene composites were prevented and that the regular layer spacings of graphene sheets were also decreased due to the insertion of Cu_2O [38,39].

Fig. 3a shows the FT-IR spectra of Cu_2O, GO, and rGO-Cu_2O. In the case of GO, a broad peak at 3400 cm^{-1} and a peak at 1730 cm^{-1} were contributed to the hydroxyl groups (-OH) and the carboxyl group (C═O), respectively. The peak at 1050 cm^{-1} corresponded to the epoxy groups (C—O) of GO. The C—C and C═C bending vibrations at 1420 and 1629 cm^{-1} were also observed [40]. For rGO-Cu_2O nanocomposites, the C═C vibration of graphene skeleton was observed at 1589 cm^{-1}. The Cu—O vibration peak (Cu_2O curve) also appeared on the line of rGO-Cu_2O nanocompos-

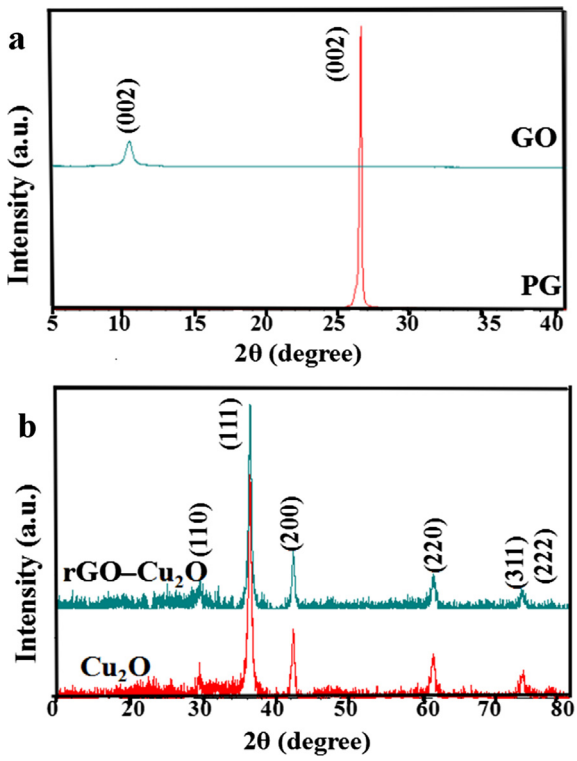

Fig. 2. XRD patterns of pristine graphite (PG) and graphene oxide (GO) (a), rGO-Cu_2O nanocomposites and Cu_2O nanoparticles (b).

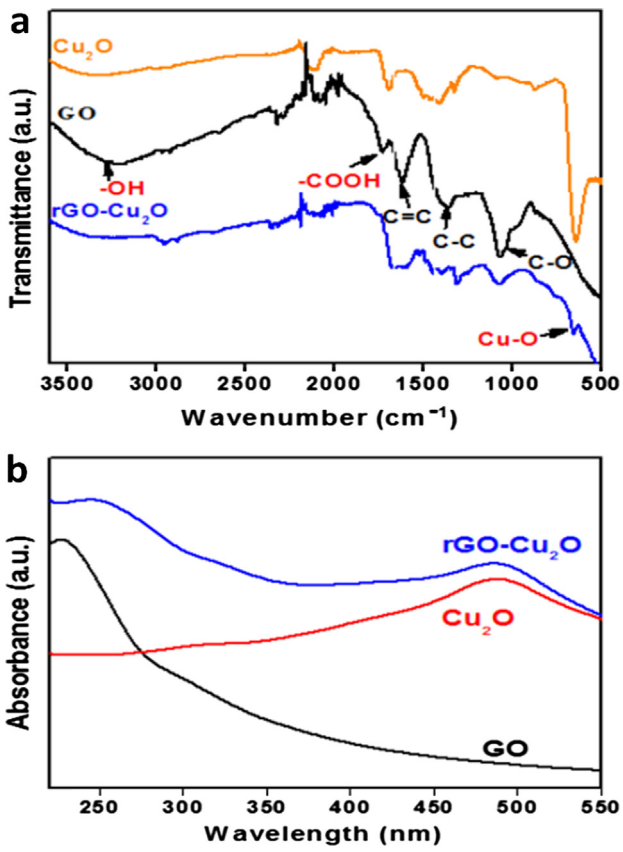

Fig. 3. FT-IR spectra (a) and UV–vis absorption spectra (b) of Cu_2O, GO, and rGO-Cu_2O.

ites, which confirmed the successful formation of the rGO and Cu_2O.

UV–vis spectroscopy was used to monitor the formation of Cu_2O nanoparticles and rGO-Cu_2O nanocomposites. Fig. 3b shows the UV–vis absorption spectra of rGO-Cu_2O, Cu_2O and GO. A characteristic absorption peak was observed in the UV–vis spectrum at about 236 nm for the π-π^* absorption band of GO [41,42] and a wide absorbing peak at 480 nm for Cu_2O [43]. The absorption peak of rGO-Cu_2O nanocomposites was similar to that of pure Cu_2O nanoparticles, while it presented a higher absorbing intensity. In addition, the characteristic absorption peak of graphene in the nanocomposites red shifted from 236 to 270 nm, confirming that the electronic conjugation within graphene nanosheets was recovered after the reduction of GO during the process of formation rGO-Cu_2O nanocomposites [41,42].

The composition of GO and rGO-Cu_2O was further confirmed by XPS spectra in Fig. 4. Fig. 4a displays the whole spectrum of rGO-Cu_2O composites which revealed the existence of Cu_2O and rGO. The XPS spectrum of Cu 2p in Fig. 4b shows two sharp peaks at 932.2 and 952.3 eV which correspond to Cu $2p_{3/2}$ and Cu $2p_{1/2}$ of Cu^+, respectively [44]. Moreover, Fig. 4b shows no peaks belonging to Cu^{2+}, indicating the high purity of the Cu_2O of the prepared rGO-Cu_2O nanocomposites. Fig. 4c shows the C 1 s high resolution spectra of rGO-Cu_2O and the corresponding quantitative deconvolution peaks. The peak at 284.7 eV corresponds to the nonoxygenated sp^2-hybridized carbon atoms C—C (C=C), another peak centered at 286.2 eV is attributed to the C—O bonds, and other peaks at 288.3 eV correspond to the C=O (carbonyl). [45]. Whereas the C 1 s XPS spectrum of GO in Fig. 4d exhibits the same oxygen functionalities, their peak intensities are stronger than those in rGO, indicating that GO has been reduced partially during the process of preparing rGO-Cu_2O nanocomposites.

The morphology of GO, Cu_2O and rGO-Cu_2O had been characterized by TEM. Fig. 5a reveals an almost-transparent single layer GO nanosheet which possesses large area. There were many wrinkles on the surface of GO to reduce the surface energy which made it more stable [46]. The size of Cu_2O nanoparticles was less than 30 nm as shown in Fig. 5b. Fig. 5c displays monodispersed cubic-like Cu_2O nanoparticles dispersed on the surface of rGO nanosheets uniformly. Zeta potential data (Fig. 5d) suggests that GO possessed strong negative charge of −51.64 mV that made GO highly stable in aqueous solutions, while Cu_2O exhibited opposite charge of 16.08 mV. Therefore, Cu_2O nanoparticles can be anchored on the surface of rGO firmly due to the electrostatic effect between rGO supports and Cu_2O nanoparticles. These results indicated that rGO nanosheets had a vital influence on the process of nucleation and stabilization.

3.2. Stability and copper ions release behavior of Cu_2O nanoparticles and rGO-Cu_2O nanocomposites

To investigate the stability, the GO, Cu_2O, and rGO-Cu_2O were dispersed in ultrapure water for different durations. Fig. 6 manifests that most Cu_2O nanoparticles began to aggregate in order to reduce specific surface energy and displayed poor dispersion after 7 days. However, rGO-Cu_2O can maintain good dispersion until 14 days. These phenomena can be explained from two aspects. Large surface area of rGO nanosheets promoted Cu_2O nanoparticles deposit on both sides of such sheets. Moreover, abundant polar functional groups such as hydroxyl, and carbonyl groups on the rGO sheet can endow rGO with excellent water solubility and firmly fix Cu_2O nanoparticles on the surface of rGO. Therefore, the aggregation problem of Cu_2O nanoparticles can be minimized and even prevented.

Copper ion release behavior has a significant impact on the bactericidal effect of Cu_2O [13]. Cu_2O nanoparticles collapsed easily and the Cu^+ ions released from Cu_2O nanoparticles had a high level under acidic environment as shown in Eq. (2) [47]. Meanwhile, as shown in Eq. (3), Cu_2O was easily oxidized to CuO by dissolved oxygen [48]. Under acidic conditions, Cu^+ ions were oxidized by

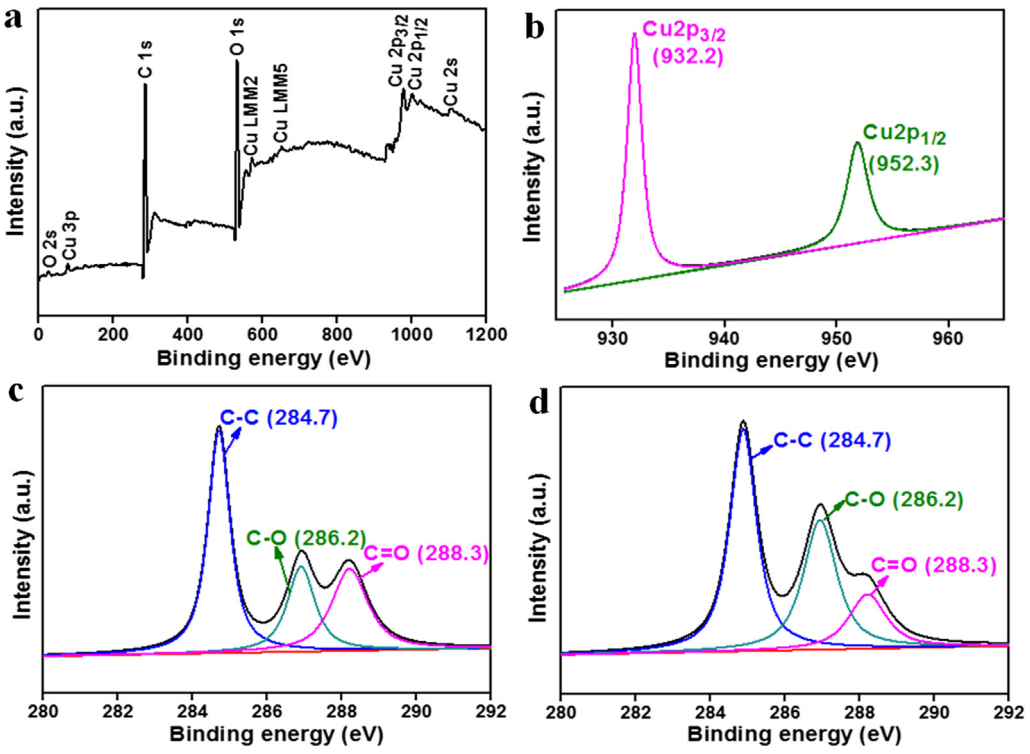

Fig. 4. The whole XPS spectrum of rGO-Cu_2O (a), XPS spectra of Cu 2p (b) and C 1 s in rGO-Cu_2O (c), XPS spectrum of C 1 s in GO (d).

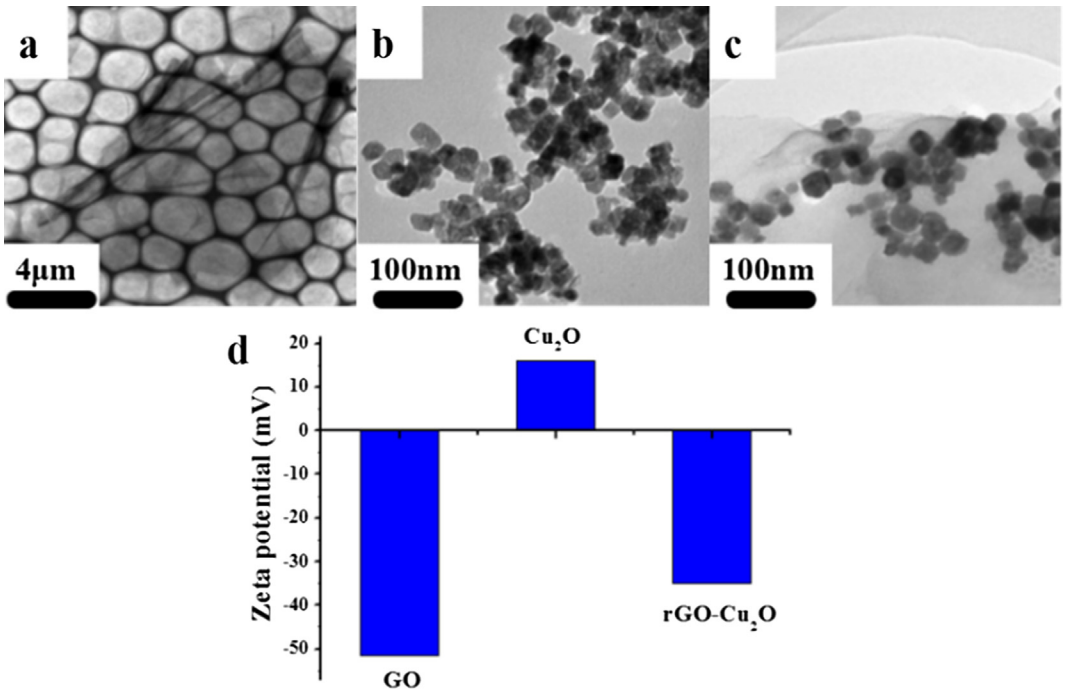

Fig. 5. TEM image of GO (a), Cu_2O nanoparticles (b) and rGO-Cu_2O nanocomposites (c); and the zeta potential of GO, Cu_2O and rGO-Cu_2O (d).

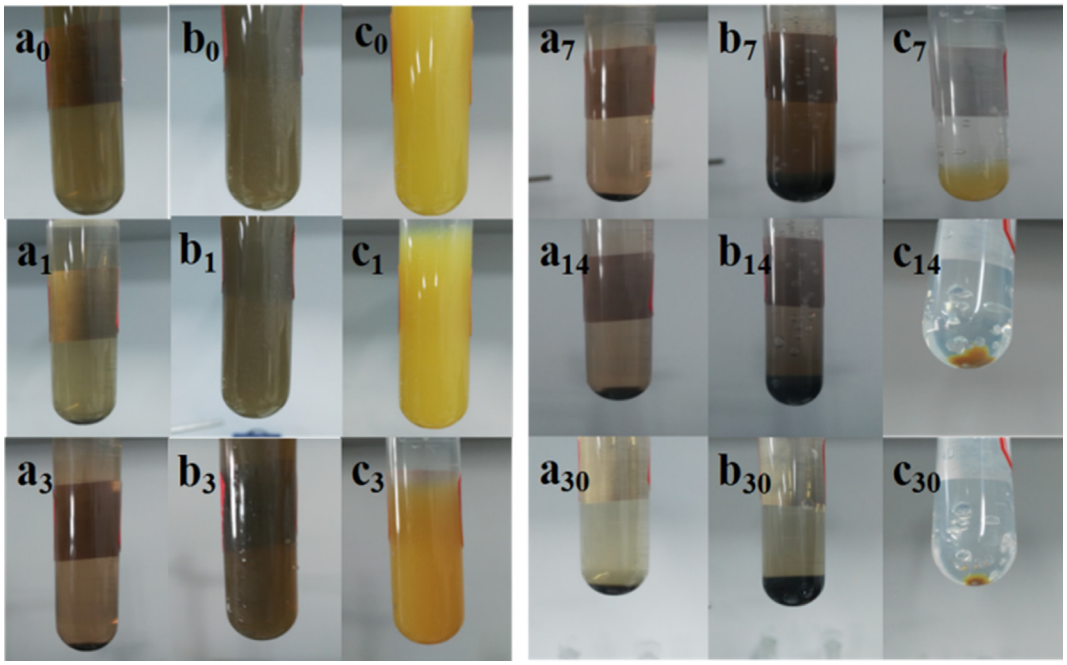

Fig. 6. Digital pictures of dispersion of GO (a_0, a_1, a_3, a_7, a_{14}, a_{30}), rGO-Cu_2O (b_0, b_1, b_3, b_7, b_{14}, b_{30}) and Cu_2O (c_0, c_1, c_3, c_7, c_{14}, c_{30}) after storage for 0, 1, 3, 7, 14, 30 days.

protons to Cu^{2+} and generated hydrogen because of the remarkable reducibility, which was labeled in Eq. (4). However, hydrogen was more active than copper and was oxidized into H^+ by Cu^{2+} before gathering into H_2 as shown in Eq. (5). The whole reaction process could be written as Eq. (6).

$$Cu_2O + 2H^+ \rightarrow 2Cu^+ + H_2O \quad (2)$$

$$2Cu_2O + O_2 \rightarrow 4CuO \quad (3)$$

$$2Cu^+ + 2H^+ \rightarrow 2Cu^{2+} + H_2 \uparrow \quad (4)$$

$$Cu^{2+} + H_2 \rightarrow Cu \downarrow + 2H^+ \quad (5)$$

$$3Cu_2O + O_2 + 2H^+ \rightarrow H_2O + Cu + Cu^{2+} + 4CuO \quad (6)$$

The copper ions release behaviors of Cu_2O and rGO-Cu_2O were characterized by ICP. The copper content of rGO-Cu_2O nanocomposites was calibrated by TG (Fig. S5) and the TG test showed that the remaining mass fractions of rGO and rGO-Cu_2O after being heated to 800 °C in nitrogen were 41.2% and 81.7%, respectively. Therefore, the mass fraction of Cu_2O in rGO-Cu_2O was 68.88% and the ICP curve of rGO-Cu_2O nanocomposites was based on the

copper content of 68.88%. As can be observed in Fig. 7, the copper ions release rate of Cu_2O nanoparticles was more rapid than that of the rGO-Cu_2O nanocomposites. Therefore, the rGO could prolong the release time of copper ions to improve the long-term bacteriostasis because rGO wrapped the Cu_2O tightly to form a protective barrier by electrostatic interaction (Fig. 5d) and reduced the possibility of Cu_2O contacting with external solution to react, as shown in Eq. (6) [49].

3.3. ROS production of rGO, Cu_2O nanoparticles and rGO-Cu_2O nanocomposites

The ROS is one of the important underlying physicochemical mechanisms leading to the toxicity of Cu_2O to microorganism [50]. As a P-type semiconductor, the electron-hole pairs of Cu_2O were separated easily under light conditions to oxidize and degrade organic materials. The reactive oxygen species assay kit was used to assess the ROS production of rGO, Cu_2O and rGO-Cu_2O stored in PBS for different time. As exhibited in Fig. 8a0, 8b0 and 8c0, the fresh rGO-Cu_2O nanocomposites generated abundant ROS, which was much more than that produced by fresh rGO and Cu_2O [51,52]. It indicated that the separation efficiency of photoexcited charges of Cu_2O was improved significantly after Cu_2O combining with rGO, because there was a better interfacial charge transfer between Cu_2O and rGO. With the increase of storage time, the performance of all kinds of samples producing ROS was restrained (Fig. 8a0-8a30, Fig. 8b0-8b30, Fig. 8c0-8c30). Especially, Cu_2O did not generate ROS thoroughly after 3 days of storage (Fig. 8c3). This may be due to the fact that lots of copper ions were released from the whole crystal surface of nanocrystals (Fig. 7), which dramatically destroyed the Cu_2O semiconductor structures and unique atom arrangements of nanocrystals, causing the failure of Cu_2O to generate ROS [14]. Nevertheless, Fig. 8b30 showed that there was still a little bit of ROS for the rGO-Cu_2O nanocomposites after immersing for 30 days. This was possibly attributed to that the rGO encased on the outside of Cu_2O nanoparticles reduced the probability of Cu_2O reacting with the external solution directly. Fig. 8b0-8b30 and Fig. 8c0-8c30 also indicate that the copper content in both samples displayed a downward trend with increasing the immersing time, while the copper content in pure Cu_2O nanoparticles decreased more violently. The changes of the atomic ratio between copper and oxygen of two samples confirmed the view that the copper ions were released from the Cu_2O crystal, which destroyed the Cu_2O semiconductor structures and

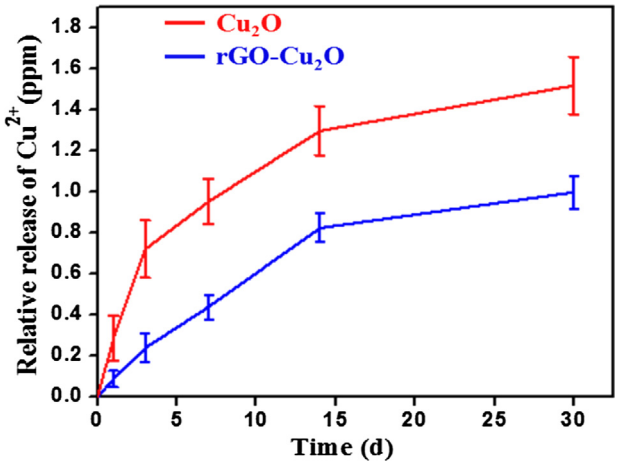

Fig. 7. The relative copper ions release curves of Cu_2O and rGO-Cu_2O after 1 day, 3 days, 7 days, 14 days, 30 days, respectively. All samples were tested at least three times.

restrained the generation of ROS. However, the copper content in the rGO-Cu_2O nanocomposites was reduced mildly, showing that rGO-Cu_2O nanocomposites could release copper ions slowly and remain stable structure in a relatively long time to generate ROS for bacteria inactivation.

To get insight into the ROS antibacterial mechanism of materials, photoluminescence (PL) spectra were conducted to study the optical properties of rGO-Cu_2O nanocomposites. Fig. 9a displays the PL spectra of Cu_2O and rGO-Cu_2O under 325 nm excitation. It was observed that the emission peak intensity of the rGO-Cu_2O nanocomposites was significantly decreased in comparison with that of Cu_2O. These results indicated that the incorporation of rGO can effectively prevent the recombination of electron-hole pairs of Cu_2O and can maintain its high photocatalytic disinfection.

Considering the discussions above, the ROS antibacterial mechanism about rGO-Cu_2O nanocomposites was similar to the mechanism of photocatalysis [53,54], which was exhibited in Fig. 9b. The photoinduced electron (e^-) preferentially transferred from Cu_2O to rGO, which could effectively suppress the recombination of electron-hole pairs, because the Fermi potential level of rGO (−4.42 eV) was lower than the conduction band (CB) of Cu_2O (−1.14 eV) [55]. The photoexcited electrons and holes of Cu_2O can directly attack the bacterial cells themselves [31]. Moreover, the rGO, playing an important role, accepted the photoexcited electrons from Cu_2O, leading to abundant photoexcited electrons on rGO surface, which provide better charge transfer between bacteria and rGO-Cu_2O nanocomposites [56,57]. The photoexcited electrons and holes induced the excess accumulation of intracellular ROS, such as hydrogen peroxide (H_2O_2), superoxide anions ($\cdot O_2^-$) or hydroxyl radicals (·OH). The abundant active substances of ROS induced nucleic acids damage, intracellular protein inactivation, dysfunction of the mitochondria, and gradual disintegration of the cell membrane leading to the cell death [58].

3.4. Antibacterial assay of Cu_2O nanoparticles and rGO-Cu_2O nanocomposites

Plate colony counting method detected the long-term antibacterial activities of rGO-Cu_2O and Cu_2O, which were stored in PBS for 0 day, 1 day, 3 days, 7 days, 14 days and 30 days, respectively. The number of *E. coli* and *S. aureus* colonies results could be seen at Fig. 10a and 10c, and the bacteriostasis of *E. coli* and *S. aureus* could be observed in Fig. 10b and 10d. As shown in Fig. 10a and 10c, the number of *E. coli* and *S. aureus* colonies exhibited an increase trend for both samples with increasing the storage time. Corresponding to the change of colonies' profile, Fig. 10b and d demonstrate that the bacteriostasis of Cu_2O nanoparticles decreased more sharply than that of rGO-Cu_2O nanocomposites for *E. coli* as well as *S. aureus*. It can be explained from two aspects why the antibacterial performance of both samples showed a downward trend during the whole storage period. Two kinds of samples reacted with O_2 and H^+ in the PBS solution to promote the Cu_2O to release copper ions (Fig. 7, Eq. (6)), destroying the regular crystal structure of cubic Cu_2O and impacting the production of ROS which was generated on a specific face mainly (Fig. 8b0-8b30, 8c0-8c30) [14]. With increasing the soaking time, these two kinds of samples agglomerated to reduce the specific surface area which reduced the probability of contacting with bacteria. However, the antibacterial effect of the rGO-Cu_2O nanocomposites was better than that of Cu_2O during the whole period. Firstly, rGO enveloped outside of the Cu_2O by electrostatic action (Fig. 5d) reduced the chance of Cu_2O contacting with the PBS solution, which slowed down the release of copper ions (Fig. 7). Secondly, rGO could improve the separation efficiency of electron-hole pairs of Cu_2O to produce more ROS to kill bacteria (Fig. 8b0-8b30, Fig. 9). Thirdly, the "blade like edges" of rGO-Cu_2O nanocomposites could

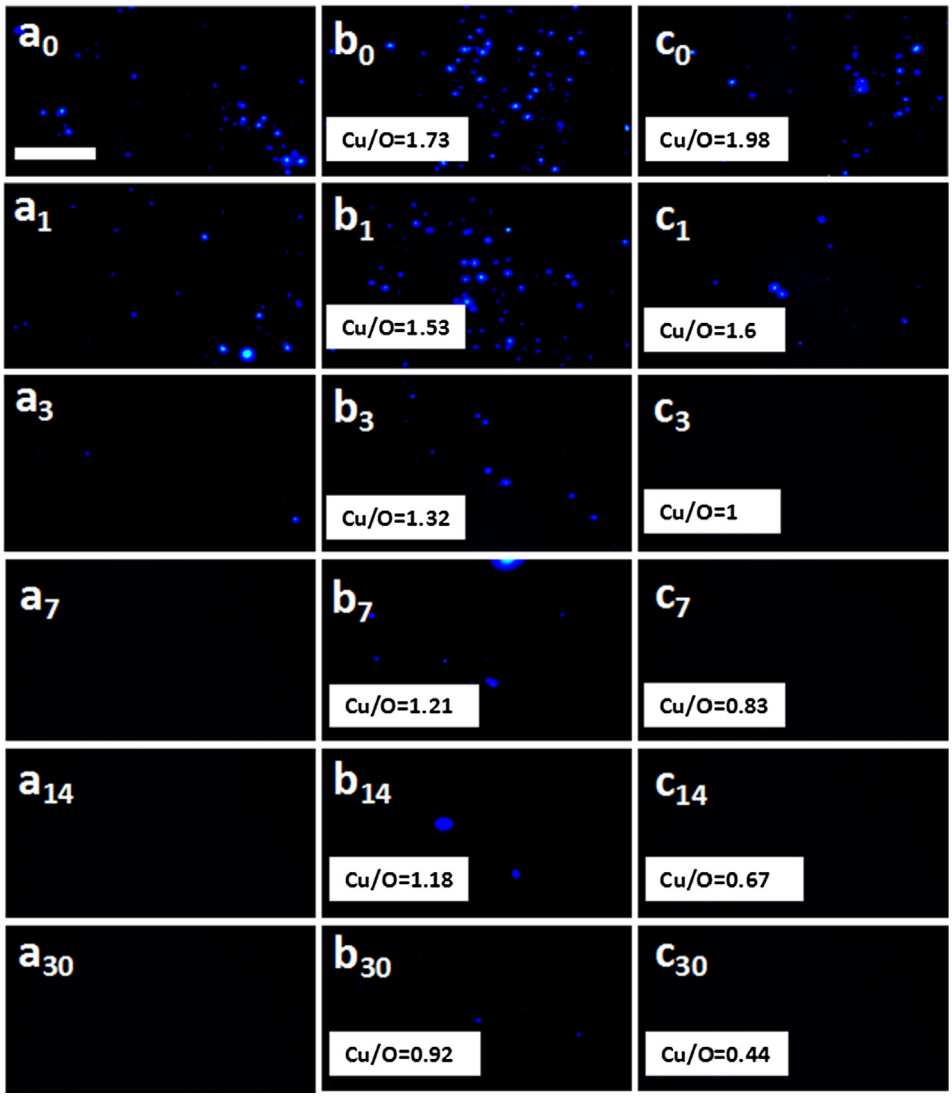

Fig. 8. ROS generation of 40 μg/mL rGO (a_0, a_1, a_3, a_7, a_{14}, a_{30}), rGO-Cu_2O (b_0, b_1, b_3, b_7, b_{14}, b_{30}) and Cu_2O (c_0, c_1, c_3, c_7, c_{14}, c_{30}) after storage for 0, 1, 3, 7, 14, 30 days, respectively. The atomic ratios between copper and oxygen of rGO-Cu_2O (b_0, b_1, b_3, b_7, b_{14}, b_{30}) and Cu_2O (c_0, c_1, c_3, c_7, c_{14}, c_{30}) after storage for 0, 1, 3, 7, 14, 30 days were analyzed using energy dispersive spectrometer (EDS), respectively. Note: Scale bar = 100 μm.

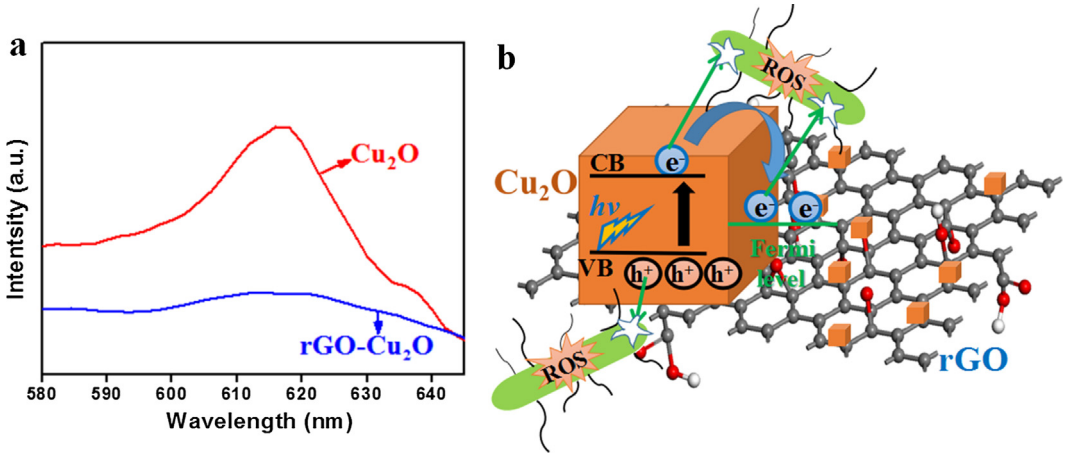

Fig. 9. PL spectra of Cu_2O nanoparticles and rGO-Cu_2O nanocomposites at the excitation wavelength of 325 nm (a). Schematic illustration of the mechanism of ROS production of rGO-Cu_2O nanocomposites (b).

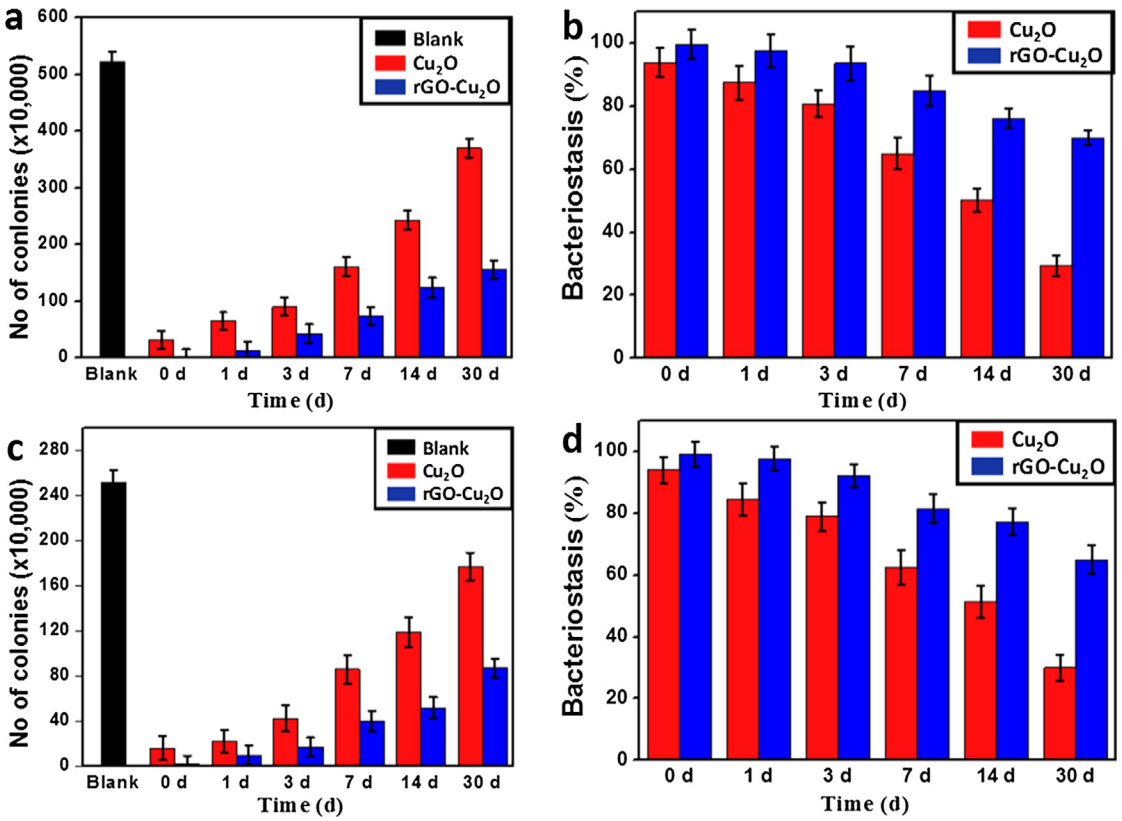

Fig. 10. The number of *E. coli* and *S. aureus* colonies in LB medium for 18 hrs containing Cu_2O and rGO-Cu_2O, which were shaken in PBS for 0 day, 1 day, 3 days, 7 days, 14 days and 30 days, respectively (a and c). The bacteriostasis of *E. coli* and *S. aureus* of Cu_2O and rGO-Cu_2O after shaking in PBS for 0 day, 1 day, 3 days, 7 days, 14 days and 30 days, respectively (b and d). All samples were tested at least three times.

destroy the bacterial cells, making the copper ions react with cytoplasmic constituents more conveniently, and finally inactivate the bacteria [33]. Fourthly, rGO can prevent Cu_2O nanoparticles from agglomerating after long time storage, rGO-Cu_2O nanocomposites possessed a larger contact area with bacteria consequently (Fig. 6-b0-6b30, 6c0-6c30), which was more conducive to kill bacteria.

The 7th day was selected as the demarcation point to further study the long-term antibacterial properties of Cu_2O nanoparticles and rGO-Cu_2O nanocomposites. As illustrated in Fig. 10b and 10d, when these two samples were stored in PBS for less than 7 days, compared with the Cu_2O nanoparticles, the antibacterial performance of the rGO-Cu_2O nanocomposites was increased by 13% and 14% against *E. coli and S. aureus*, respectively. Although the dispersibility of these two samples was not significantly different, the ROS generation ability and the copper ions release rate were very different within 7 days. The Cu_2O nanoparticles did not generate ROS on the third day, while the rGO-Cu_2O nanocomposites could generate ROS continuously during this time (Fig. 8b0-8b3, 8c0-8c3). In addition, the Cu_2O nanoparticles had a tendency of releasing copper ions within 7 days quickly (Fig. 7). Hence, the antibacterial properties of Cu_2O nanoparticles were suppressed more severely than those of the rGO-Cu_2O nanocomposites. When the storage time was over 7 days, the antibacterial performance of rGO-Cu_2O nanocomposites was far better than that of Cu_2O nanoparticles. The bacteriostasis of Cu_2O nanoparticles against *E. coli and S. aureus* dropped to 29.33% and 31.03% respectively at the 30th day, whereas rGO-Cu_2O nanocomposites still displayed a strong antibacterial activity, which possessed 70.09% and 65.06%, respectively. The bactericidal effect of ROS of both samples was not apparent over 7 days, although the rGO-Cu_2O nanocomposites could still produce small amount of ROS on the 30th day. Because the release of copper ions of two samples destroyed the Cu_2O semiconductor structures, however, the rGO could protect the internal Cu_2O from reacting with O_2 and H^+ too quickly and remain its stable structure in a relatively long time (Fig. 8b7-8b30, 8c7-8c30). The difference of antibacterial effect between Cu_2O nanoparticles and rGO-Cu_2O nanocomposites was mainly attributed to the copper ion release properties and dispersibility after storage in PBS over 7 days. The rGO-Cu_2O nanocomposites still keep prominent copper ions sterilization effect by retarding the release of copper ions and reducing the mass loss of Cu_2O (Fig. 7) [59]. Furthermore, the dispersibility of Cu_2O nanoparticles had been enhanced after Cu_2O combining with rGO which possessed excellent solubility by electrostatic interaction, improving the contact area with bacteria consequently (Fig. 6b7-6b30, 6c7-6c30). Therefore, the prepared rGO-Cu_2O nanocomposites possessed high efficient sterilization because of the synergistic effect of sustained release of copper ions, elevated ROS production ability and excellent dispersion of rGO-Cu_2O nanocompositesthe.

4. Conclusion

This work provides a novel facile strategy to design stable rGO-Cu_2O nanocomposites utilizing the electrostatic interaction and special electronic transition between rGO and Cu_2O, presenting formidable antibacterial capacity and long-term effectiveness [26,60]. As a result, the monodispersed Cu_2O nanoparticles with a size of 25 nm were dispersed well on the surface of rGO nanosheets. The antibacterial test results indicated that the rGO-Cu_2O nanocomposites presented powerful long-lasting antibacterial capability against *E. coli* and *S. aureus*. As systematically revealed by stability test, copper ion release test and ROS

detection, the enhanced antibacterial mechanisms of rGO-Cu_2O nanocomposites were due to the synergistic effect of sustained release of copper ions, elevated ROS production ability and excellent dispersion of rGO-Cu_2O nanocomposites. The specific findings can be summarized as follows: (1) Initially, the rGO wrapped the Cu_2O by electrostatic interaction, protecting Cu_2O from reacting with external solution directly, which extended the release period of copper ions; (2) The sharp edges of rGO nanosheets can damage the bacterial cell membranes physically, making the copper ions react with bacterial cell more conveniently, which maintained a highly efficient ion sterilization; (3) Furthermore, the rGO-Cu_2O nanocomposites had a stronger ROS generation capacity and a longer ROS generation time than pure Cu_2O due to the fact that the rGO promoted the charge carrier separation of Cu_2O and protected Cu_2O from falling apart quickly in PBS solution; 4) Finally, the dispersibility of rGO-Cu_2O nanocomposites had been improved in aqueous solution owing to the excellent solubility of rGO, thus the prepared bactericide had a larger contacting surface with bacteria to kill bacteria. The produced rGO-Cu_2O is a promising bactericide in the antibacterial fields and can provide an alternative strategy for fighting against drug-resistance crisis in public health. We hope to further optimize the process of preparing materials or combine Cu_2O with other materials to synthesize more efficient and environmental friendly long-term fungicides.

Acknowledgements

This work was supported by the National Natural Science Foundation (51572249), the Natural Science Foundation for Shandong Province (ZR2014EMM021, ZR2017MD016) and the Fundamental Research Funds for the Central Universities (841562011).

References

[1] A.F.D. Faria, D.S.T. Martinez, S.M.M. Meira, A.C.M.D. Moraes, A. Brandelli, A.G.S. Filho, O.L. Alves, Anti-adhesion and antibacterial activity of silver nanoparticlessupported on graphene oxide sheets, Colloid. Surface. B. 113 (2014) 115–124.
[2] P. Madhavan, P.Y. Hong, R. Sougrat, S.P. Nunes, Silver-enhanced block copolymer membranes with biocidal activity, ACS Appl. Mater. Interf. 6 (2014) 18497–18501.
[3] M.C. Wu, A.R. Deokar, J.H. Liao, P.Y. Shih, Y.C. Ling, Graphene-based photothermal agent for rapid and effective killing of bacteria, ACS Nano 7 (2013) 1281–1290.
[4] P.V. AshaRani, G.L.K. Mun, M.P. Hande, S. Valiyaveettil, Cytotoxicity and genotoxicity of silver nanoparticles in human cells, ACS Nano 3 (2009) 279–290.
[5] R.J. Barnes, R. Molina, J. Xu, P.J. Dobson, I.P. Thompson, Comparison of TiO_2 and ZnO nanoparticles for photocatalytic degradation of methylene blue and the correlated inactivation of gram-positive and gram-negative bacteria, J. Nanopart. Res. 15 (2013) 1432–1443.
[6] Z. Luo, Q. Wu, J. Xue, Y. Ding, Selectively enhanced antibacterial effects and ultraviolet activation of antibiotics with ZnO nanorods against Escherichia Coli, J. Biomed. Nanotechnol. 9 (2013) 69–76.
[7] M.M. Momeni, Y. Ghayeb, M. Menati, Facile and green synthesis of CuO nanoneedles with high photo catalytic activity, J. Mater. Sci-Mater. El. 27 (2016) 9454–9460.
[8] J. Lv, C. Kong, X. Hu, X. Zhang, K. Liu, S. Yang, J. Bi, X. Liu, G. Meng, J. Li, Z. Yang, S. Yang, Zinc ion mediated synthesis of cuprous oxide crystals for non-enzymatic glucose detection, J. Mater. Chem. B 5 (2017) 8686–8694.
[9] X. Han, X. He, F. Wang, J. Chen, J. Xu, X. Wang, X. Han, Engineering an N-doped Cu_2O@N-C interface with long-lived photo-generated carriers for efficient photoredox catalysts, J. Mater. Chem. A 5 (2017) 10220–10226.
[10] M.M. Momeni, M. Mirhosseini, Z. Nazari, A. Kazempour, M. Hakimiyan, Antibacterial and photocatalytic activity of CuO nanostructure films with different morphology, J. Mater. Sci-Mater. El. 27 (2016) 8131–8137.
[11] M.M. Momeni, M. Mirhosseini, N. Mohammadi, Fabrication, Efficient photo catalytic degradation of methyl orange over Ag-CuO nanostructures grown on copper foil under visible light irradiation, J. Mater. Sci-Mater. El. 27 (2016) 6542–6551.
[12] M.M. Momeni, N. Mohammadi, M. Mirhosseini, Photo catalytic property of Pt-CuO nanostructure films prepared by wet-chemical route and photochemical deposition method, J. Mater. Sci-Mater. El. 7 (2016) 10147–10156.
[13] S.L. Warnes, C.W. Keevil, Mechanism of Copper surface toxicity in vancomycin-resistant enterococci following wet or dry surface contact, Appl. Environ. Microb. 77 (2011) 6049–6059.
[14] Y. Feng, Y. Chang, X. Sun, N. Liu, Y. Chang, Y. Feng, H. Zhang, X. Li, Understanding the property-activity relationships of polyhedral cuprous oxide nanocrystals in terms of reactive crystallographic facets, Toxicol. Sci. 156 (2017) 480–491.
[15] Z. Sun, D.K. James, J.M. Tour, Graphene chemistry: synthesis and manipulation, J. Phys. Chem. Lett. 2 (2011) 2425–2432.
[16] X. Hao, S. Chen, H. Zhu, L. Wang, Y. Zhang, Y. Yin, The synergy of graphene oxide and polydopamine assisted immobilization of lysozyme to improve antibacterial properties, ChemistrySelect 2 (2017) 2174–2182.
[17] H. Chen, M.B. Müller, K.J. Gilmore, G.G. Wallace, D. Li, Mechanically strong, electrically conductive, and biocompatible graphene paper, Adv. Mater. 20 (2008) 3557–3561.
[18] X. Hao, S. Chen, H. Yu, D. Liu, W. Sun, Metal ion-coordinated carboxymethylated chitosan grafted carbon nanotubes with enhanced antibacterial properties, RSC Adv. 6 (2016) 39–43.
[19] J. Zhao, S. Pei, W. Ren, L. Gao, H.M. Cheng, Efficient preparation of large-area graphene oxide sheets for transparent conductive films, ACS Nano 4 (2010) 5245–5252.
[20] X. Hao, S. Chen, W. Wang, Z. Yang, L. Yue, H. Sun, F. Cheng, AgNP-coordinated glucosamine-grafted carbon nanotubes with enhanced antibacterial properties, New J. Chem. 41 (2017) 7045–7051.
[21] S. Stankovich, D.A. Dikin, R.D. Piner, K.A. Kohlhaas, A. Kleinhammes, Y. Jia, Y. Wu, S.T. Nguyen, R.S. Ruoff, Synthesis of graphene-based nanosheets via chemical reduction of exfoliated graphite oxide, Carbon 45 (2007) 1558–1565.
[22] Y. Wang, C. Li, T. Wu, X. Ye, Polymerized ionic liquid functionalized graphene oxide nanosheets as a sensitive platform for bisphenol A sensing, Carbon 129 (2018) 21–28.
[23] R. Mehta, S. Chugh, Z. Chen, Enhanced electrical and thermal conduction in graphene-encapsulated copper nanowires, Nano Lett. 15 (2015) 2024–2030.
[24] M. Dinari, M.M. Momeni, M. Afshari, Fabrication and characterization of hybrid films based on polyaniline and graphitic carbon nitride nanosheet, J. Appl. Polym. Sci. 133 (2016).
[25] M. Afshari, M. Dinari, M.M. Momeni, Ultrasonic irradiation preparation of graphitic-C_3N_4/polyaniline nanocomposites as counter electrodes for dye-sensitized solar cells, Ultrason. Sonoche. 42 (2018) 631–639.
[26] Q. Hen, L. Zhang, G. Chen, Facile preparation of graphene-copper nanoparticle composite by in situ chemical reduction for electrochemical sensing of carbohydrates, Anal. Chem. 84 (2012) 171–178.
[27] B. Adhikari, A. Biswas, A. Banerjee, Graphene oxide-based supramolecular hydrogels for making nanohybrid systems with Au nanoparticles, Langmuir 28 (2012) 1460–1469.
[28] N.J. Bell, Y.H. Ng, A. Du, H. Coster, S.C. Smith, R. Amal, Understanding the enhancement in photoelectrochemical properties of photocatalytically prepared TiO_2-reduced graphene oxide composite, J. Phys. Chem. C 115 (2011) 6004–6009.
[29] W. Shao, X. Liu, H. Min, G. Dong, Q. Feng, S. Zuo, Preparation, characterization, and antibacterial activity of silver nanoparticle-decorated graphene oxide nanocomposite, ACS Appl. Mater. Interf. 7 (2015) 6966–6973.
[30] Y. Lei, F. Chen, R. Li, J. Xu, A facile solvothermal method to produce graphene-ZnS compositesfor superior photoelectric applications, Appl. Surf. Sci. 308 (2014) 206–210.
[31] R. Wang, X. Kong, W. Zhang, W. Zhu, L. Huang, J. Wang, X. Zhang, X. Liu, N. Hu, Y. Suo, J. Wang, Mechanism insight into rapid photocatalytic disinfection of Salmonella based on vanadate QDs-interspersed g-C_3N_4 heterostructures, Appl. Catal. B-Environ. 225 (2018) 228–237.
[32] K.S. Hui, K.N. Hui, D.A. Dinh, C.H. Tsang, Y.R. Cho, W. Zhou, X. Hong, H.H. Chun, Green synthesis of dimension-controlled silver nanoparticle–graphene oxide with in situ ultrasonication, Acta Mater. 64 (2014) 326–332.
[33] X. Cai, M. Lin, S. Tan, W. Mai, Y. Zhang, Z. Liang, Z. Lin, X. Zhang, The use of polyethyleneimine-modified reduced graphene oxide as a substrate for silver nanoparticles to produce a material with lower cytotoxicity and long-term antibacterial activity, Carbon 50 (2012) 3407–3415.
[34] D.C. Marcano, D.V. Kosynkin, J.M. Berlin, A. Sinitskii, Z. Sun, A. Slesarev, L.B. Alemany, W. Lu, J.M. Tour, Improved Synthesis of Graphene Oxide, ACS Nano 4 (2010) 4806–4814.
[35] L. Gou, C.J. Murphy, Controlling the size of Cu_2O nanocubes from 200 to 25 nm, J. Mater. Chem. 14 (2004) 735–738.
[36] Y. Deng, J. Zhao, Q. Li, X. Xu, H. Lin, Y. Li, A generic in situ seed-mediated size-control method in the case of cuprous oxide nanocubes and their antibacterial activities, CrystEngComm 16 (2014) 5184–5188.
[37] S. Liu, T. Zeng, M. Hofmann, E. Burcombe, J. Wei, R. Jiang, J. Kong, Y. Chen, Antibacterial activity of graphite, graphite oxide, graphene oxide, and reduced graphene oxide: membrane and oxidative stress, ACS Nano 5 (2011) 6971–6980.
[38] M.Y. Wang, J.R. Huang, Z.W. Tong, W.H. Li, J. Chen, Reduced graphene oxide-cuprous oxide composite via facial deposition for photocatalytic dye-degradation, J. Alloy. Compd. 568 (2013) 26–35.
[39] Z. Gao, J. Wang, Z. Li, W. Yang, B. Wang, M. Hou, Y. He, Q. Liu, T. Mann, P. Yang, M. Zhang, L. Liu, Graphene nanosheet/Ni^{2+}/Al^{3+} layered double-hydroxide composite as a novel electrode for a supercapacitor, Chem. Mater. 23 (2011) 3509–3516.
[40] Y. Zhou, G. Chen, Y. Yu, L. Hao, Z. Han, Q. Yu, Oxygen functional groups induced formation of Cu_2O nanoparticles on the surface of reduced graphene oxide, New J. Chem. 37 (2013) 2845–2850.

[41] T. Kavinkumar, K. Varunkumar, V. Ravikumar, S. Manivannan, Anticancer activity of graphene oxide-reduced graphene oxide-silver nanoparticle composites, J. Colloid. Interf. Sci. 505 (2017) 1125–1133.
[42] P. Thangavel, R. Kannan, B. Ramachandran, G. Moorthy, G. Suguna, V. Muthuvijayan, Development of reduced graphene oxide (rGO)-isabgol nanocomposite dressings for enhanced vascularization and accelerated wound healing in normal and diabetic rats, J. Colloid. Interf. Sci. 517 (2018) 251–264.
[43] J. Ma, S. Guo, X. Guo, H. Ge, Preparation, characterization and antibacterial activity of core-shell Cu_2O@Ag composites, Surf. Coat. Tech. 272 (2015) 268–272.
[44] M.A. Nguyen, N.M. Bedford, Y. Ren, E.M. Zahran, R.C. Goodin, F.F. Chagani, L.G. Bachas, M.R. Knecht, Direct synthetic control over the size, composition, and photocatalytic activity of octahedral copper oxide materials: correlation between surface structure and catalytic functionality, ACS Appl. Mater. Interf. 7 (2015) 13238–13250.
[45] Y. Ma, X. Li, Z. Yang, S. Xu, W. Zhang, Y. Su, N. Hu, W. Lu, J. Feng, Y. Zhang, Morphology control and photocatalysis enhancement by in situ hybridization of cuprous oxide with nitrogen-doped carbon quantum dots, Langmuir 32 (2016) 9418–9427.
[46] F. Zhang, Y. Li, Y. Gu, Z. Wang, C. Wang, One-pot solvothermal synthesis of a Cu_2O/graphene nanocomposite and its application in an electrochemical sensor for dopamine, Microchim. Acta 173 (2011) 103–109.
[47] Y. Wang, T. Gao, K. Wang, X. Wu, X. Shi, Y. Liu, S. Luo, S. Zhou, Template-assisted synthesis of uniform nanosheet-assembled silver hollow microcubes, Nanoscale 4 (2012) 7121–7126.
[48] C. Cai, T. Zhu, D. Li, Y. Ran, H. Dong, N. Zhao, J. Xu, Spherically aggregated Cu_2O-TA hybrid submicroparticles with modulated size and improved chemical stability, CrystEngComm 19 (2017) 1888–1895.
[49] M.M. Momeni, Y. Ghayeb, M. Menat, Characterization and photoelectrochemical properties of cuprous oxide-reduced graphene oxide photocatalysts for hydrogen generation, J. Mater. Sci-Mater. El. 29 (2018) 4136–4146.
[50] W. Fan, X. Wang, M. Cui, D. Zhang, Y. Zhang, T. Yu, L. Guo, Differential oxidative stress of octahedral and cubic Cu_2O micro/nanocrystals to daphnia magna, Environ. Sci. Technol. 46 (2012) 10255–10262.
[51] A.M. El-Saeed, M.A. El-Fattah, A.M. Azzam, M.M. Dardir, M.M. Bader, Synthesis of cuprous oxide epoxy nanocomposite as an environmentally antimicrobial coating, Int. J. Biol. Macromol. 89 (2016) 190–197.
[52] M.U. Farid, S. Jeong, D.H. Seo, R. Ahmed, C. Lau, N.K. Gali, Z. Ning, A.K. An, Mechanistic insight into the in vitro toxicity of graphene oxide against biofilm forming bacteria using laser-induced breakdown spectroscopy, Nanoscale 10 (2018) 4475–4487.
[53] M.M. Momeni, Y. Ghayeb, F. Ezati, Fabrication, Fabrication, characterization and photoelectrochemical activity of tungsten-copper co-sensitized TiO2 nanotube composite photoanodes, J. colloid interf. Sci. 514 (2018) 70–82.
[54] M.M. Momeni, Y. Ghayeb, M. Shafiei, Preparation and characterization of $CrFeWTiO_2$ photoanodes and their photoelectrochemical activities for water splitting, Dalton Trans. 46 (2017) 12527–12536.
[55] Q. Wei, Y. Wang, H. Qin, J. Wu, Y. Lu, H. Chi, F. Yang, B. Zhou, H. Yu, J. Liu, Construction of rGO wrapping octahedral Ag-Cu_2O heterostructure for enhanced visible light photocatalytic activity, Appl. Catal. B-Environ. 227 (2018) 132–144.
[56] W. Zhang, Y. Ma, Z. Yang, X. Tang, X. Li, G. He, Y. Cheng, Z. Fang, R. He, Y. Zhang, Analysis of synergistic effect between graphene and octahedral cuprous oxide in cuprous oxide-graphene composites and their photocatalytic application, J. Alloy. Compd. 712 (2017) 704–713.
[57] Y.C. Pu, H.Y. Chou, W.S. Kuo, K.H. Wei, Y.J. Hsu, Interfacial charge carrier dynamics of cuprous oxide-reducedgraphene oxide (Cu_2O-rGO) nanoheterostructures and their related visible-light-driven photocatalysis, Appl. Cataly. B-Environ. 204 (2017) 21–32.
[58] P. Choudhary, T. Parandhaman, B. Ramalingam, N. Duraipandy, M.S. Kiran, S.K. Das, Fabrication of nontoxic reduced graphene oxide protein nanoframework as sustained antimicrobial coating for biomedical application, ACS Appl. Mater. Interf. 9 (2017) 38255–38269.
[59] S. Kittler, C. Greulich, J. Diendorf, M. Koller, M. Epple, Toxicity of silver nanoparticles increases during storage because of slow dissolution under release of silver ions, Chem. Mater. 22 (2010) 4548–4554.
[60] R. Zhao, M. Lv, Y. Li, M. Sun, W. Kong, L. Wang, S. Song, C. Fan, L. Jia, S. Qiu, Y. Sun, H. Song, R. Hao, Stable nanocomposite based on PEGylated and silver nanoparticles loaded graphene oxide for long-term antibacterial activity, ACS Appl. Mater. Interf. 9 (2017) 15328–15341.